Multi-Objective Optimization of Reservoir Operation using Machine Learning Models. Case study: Hatillo Reservoir in the Dominican Republic

C. Tami[1], G. Corzo[2], F. Perez[3], and G. Santos[1]

[1]Escuela Colombiana de Ingeniería Julio Garavito, Bogotá D.C, Colombia

[2]IHE Delft, Institute for Water Education, Delft, The Netherlands

[3]Pontificia Universidad Católica Madre y Maestra, Santo Domingo, Dominican Republic

Index terms

1857 – Reservoirs (surface), 1880 – Water management, 1906 – Computational models, algorithms, 1849 – Numerical approximations and analysis, 1847 – Modeling.

Keywords

Multipurpose Reservoirs, Reservoir Operations, Multiobjective Optimization, Machine Learning Models, Pareto Front.

Abstract

Finding optimum balances between conflicting interests in multipurpose reservoirs often represents an important challenge for decision makers. This study assesses the use of different computational tools to obtain optimal reservoir operations applied to the Hatillo dam in the Dominican Republic. A multi-objective optimization approach is used, in which non-dominated sorting genetic algorithm II (NSGAII) and multi-objective evolutionary algorithm based on decomposition (MOEA/D) optimizers are applied to models that simulate reservoir operations. Three different Machine Learning (ML) models, namely, the multilayer perceptron (MLP), the radial basis network (RBN) and the linear function (LF), are employed to learn the current operation of the system. Subsequently, a general model is proposed to simulate daily reservoir operations (2009-2019), integrating water balances, physical constraints of the dam components and the ML models, the latter defining daily controlled discharges. In the optimization process, the ML parameters are the decision variables, while the objectives evaluated are irrigation, hydropower generation and flood control. The results are compared with the actual operation of the reservoir. Three dimensional Pareto fronts are obtained, from which, the wide variety of operations can be evidenced. The flood control objective was found to have a wide room for improvement over the current operation of the reservoir, and several of the solutions found improve the current operation for the three proposed objectives. The MLP models tend to generate the best results for this case study and the NSGAII optimizer generates the best optimization results.

1 Introduction

Reservoir optimization is one of the most relevant study areas within the field of water resource systems (Momtahen & Dariane, 2007). With the effect of climate-change, population growth, and basin dynamics, optimal operation of reservoirs has more relevance in water resources management.

Multipurpose reservoirs are often used to attend multiple demands for domestic, industrial, irrigation, environment, hydropower production and flood control, among others (Sun, Luo, & Xie, 2018). Therefore, considering the different interests that may exist in decision-making for the operation of reservoirs, as well as the mutual conflicts that these interests may present, finding operating policies to which all the involved parties will agree is not an easy task. For flood control objective, for instance, it is better if there is less water in the reservoir, allowing to accumulate a large additional volume of water during the flood season (Zhou et al., 2018), while more water in the reservoir is better for irrigation purposes (Scola et al., 2014). Regarding hydropower production, the stored energy in the reservoir gradually increases with the rise in water level (Jansen et al., 2013), and outflows might support irrigation, however, there are also well-known cases where hydropower production reduces water availability for irrigation (Ruijie, Cai, Ringler, & Zhu, 2017). Thus, finding optimal operating policies that use multi-objective approaches to re-focus decision-making towards a balance of interests is highly relevant to improve the integrated use of reservoirs. It is important to address trade-offs between multiple objectives to achieve the management goals (Myo Lin & Rutten, 2016).

The literature cites different approaches for tackling multi-objective optimization problems. Many of these are oriented towards the search for sets of non-dominated solutions reflected in decision spaces or Pareto fronts. Traditional approaches aim to simplify multi-objective problems into several single-objective problems that can be addressed via standard optimization algorithms (Miettinen, 1999). For instance, the weights or weighting method converts objectives into scalar values by assigning subjective weights (Labadie, 2004), or the Ɛ-constrained method (Haimes et al., 1971) transforms all objectives into constraints except for one, to which a standard optimization method is applied, thus simplifying the problem. Both methods are widely applied in reservoir optimization (see Heydari et al., 2016; Ko et al., 1992; Khattab & Al-Mohseen, 2020). Another method, the Goal attainment (Gembicki & Haimes, 1975) consists of defining a set of specified targets associated with a set of objectives, which can be under- or overachieved, and are controlled by a vector of weighting coefficients (Loucks & van Beek, 2017). In reservoir optimization, this method has been employed by Khattab & Al-Mohseen (2020), and Basu (2004). All these approaches, however, are limited when the complexity of the problem increases (e.g., greater number of objective functions, decision variables or constraints).

Thanks to advancements in computational resources, better technologies and more robust equipment, metaheuristic techniques have been gaining popularity in the field of water resources. Such is the case for evolutionary algorithms (EA) that use the mechanisms of Darwin's evolution of species (see Cámara, 2015; Loucks & van Beek, 2017). When applied to multi-objective optimization, EAs are efficient because of their ability to solve complex problems involving characteristics such as discontinuities, multi-modality, disjoint feasible spaces and noise when evaluating functions (Ma et al., 2015). These algorithms seek to generate a Pareto-approximate set of solutions to serve as a reference for decision-making in multi-criteria problems (see Kollat et al., 2011; Giuliani et al., 2014). Among these EAs, the Non-dominated Sorting Genetic Algorithm II (NSGAII) (Deb et al., 2002) and the Multi-objective Evolutionary Algorithm Based

on Decomposition (MOEA / D) (Zhang & Li, 2007) stand out. Some authors have used these algorithms to optimize multipurpose reservoirs. Castelletti et al. (2012) used the NSGAII to optimize the Hoa Binh reservoir on the Da River in Vietnam for hydroelectric generation, water supply and flood control. Myo Lin et al. (2020) also used the NSGAII within the scope of multi-objective model predictive control for real-time operation of a multi-reservoir system in the Sittaung river basin in Myanmar. Similarly, Ma et al. (2015) applied the MOEA / D to optimize the Ankang reservoir in China for flood control.

One approach that has gained popularity in recent years is Direct Search (DS), a term attributed to Rosenstein and Barto (2001). This concept is also known in water resource literature as parameterization-simulation-optimization, as referenced by Koutsoyiannis and Economou (2003). Per this method, optimizers are applied directly to approximation functions or models that simulate the reservoir's operation (Ritter, 2016). Some recent studies have applied approximation functions or machine learning (ML) models that use artificial neural networks (ANNs) to represent reservoir operations (e.g., Ehsani et al., 2016; Zhang et al., 2018). Giuliani et al. (2014) and Giuliani et al. (2016) used radial basis networks (RBNs), demonstrating their benefits as universal approximation functions. Likewise, Ritter et al. (2020) applied DS using physically based operating models.

This study uses the Hatillo reservoir in the Dominican Republic as a case study to propose a methodology for searching for optimal operations for multipurpose reservoirs. The Hatillo reservoir has three purposes in mutual conflict: hydroelectric generation, irrigation and flood control. Under the proposed methodology, three different Machine Learning (ML) models, namely, the multilayer perceptron (MLP), the radial basis network (RBN) and the linear function (LF), are employed to learn what is (to discover) the current operation of the system. Subsequently, a general model is proposed to simulate daily reservoir operations (2009-2019), integrating water balances, physical constraints of the dam components and the ML models, the latter defining daily controlled discharges. In the optimization process, the ML parameters are the decision variables, while the objectives evaluated are irrigation, hydropower generation and flood control. The NSGAII and MOEA/D, two EAs widely applied in multi-objective problems, are used to optimize the proposed models. The results are compared with the current operation of the reservoir for the period of analysis. Both the operation models and the optimizations are created using Python.

The main contribution of this study is a proposed framework that develops optimal operations for the Hatillo reservoir to improve the current operation for the three proposed objectives. Three dimensional Pareto fronts are obtained, from which, the wide variety of operations can be evidenced, which could even serve as a reference for decision-making towards a balance of interests, thus improving the integral use of the reservoir. This methodology could be applied in multipurpose reservoirs in general, though the operation model must be adapted to each case. The study also evaluates the performance of the NSGAII and MOEA / D optimizers in searching for optimal reservoir operations, as well as the ML models used to parameterize the reservoir's operation. The following sections describe the case study and the proposed methodology, and later demonstrate the results and conclusions of the study.

2 Case Study

The Hatillo reservoir is in the Yuna river basin (Figure 1), Dominican Republic, about 113 kilometers northeast of Santo Domingo. This reservoir has been used for irrigation, hydropower

generation, and to mitigate downstream flooding. The Yuna river basin drains an area of 5,498 km^2, flowing downstream for approximately 210 kilometers. It is the second most important river in the Dominican Republic, and with an average flow of 91 m^3/s at its mouth (35.4 m^3/s at the entrance of the reservoir), it is the river with the highest flow. Mean annual precipitation in the basin (in terms of spatial variation) ranges between 1,080 and 3,120 mm, with the area of greatest precipitation in the mountain region upstream of the reservoir. Most of the annual rainfall in the Dominican Republic occurs between the end of April and the end of October, with a bimodal trend that has peaks in May and around the end of August to October (CEPAL, 2020; Jury et al., 2007). Due to its geographical location, the country is exposed to extreme weather events such as hurricanes, cyclones and tropical storms. The hurricane season begins in June and ends in November, being the months of August to the end of October the periods of greatest occurrence (Jesús Encarnación, 2019).

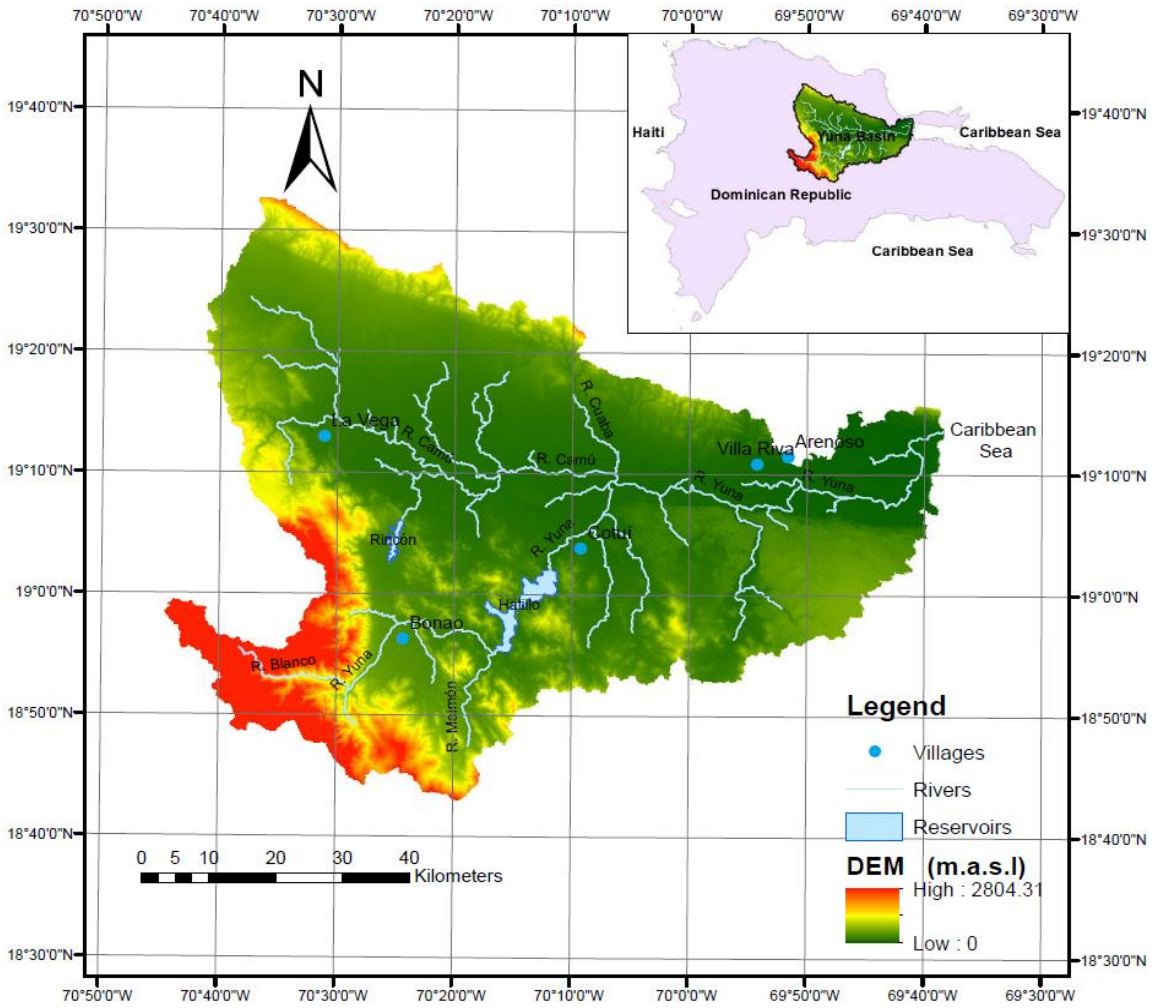

Figure 1. Map of the Yuna river basin.

During periods of prolonged rain, floods occur frequently in the lower Yuna basin. The rains generate an increase in river flow that consequently overflows and affects low-lying populations downstream of the reservoir. The lower Yuna plain is subject to flooding in general,

characterized by a terrain of low slopes, extensive plains and a meandering river course. Several flood events have been reported, such as flooding in October of 2007 that occurred because of Tropical Storm Noel. The event affected the entire Dominican territory and resulted in losses exceeding 439 million US dollars (Economic Commission for Latin America and the Caribbean, 2008). Another more recent event was the flood season between November 2016 and April 2017, which generated losses of 862.37 million US dollars, affecting sectors of public works, water and sewerage, agriculture and housing among others (MEPyD, 2017). On the other extreme, periods of long droughts also affect the area, reducing hydroelectric generation and putting at risk the water meant to supply the irrigation districts in the lower Yuna.

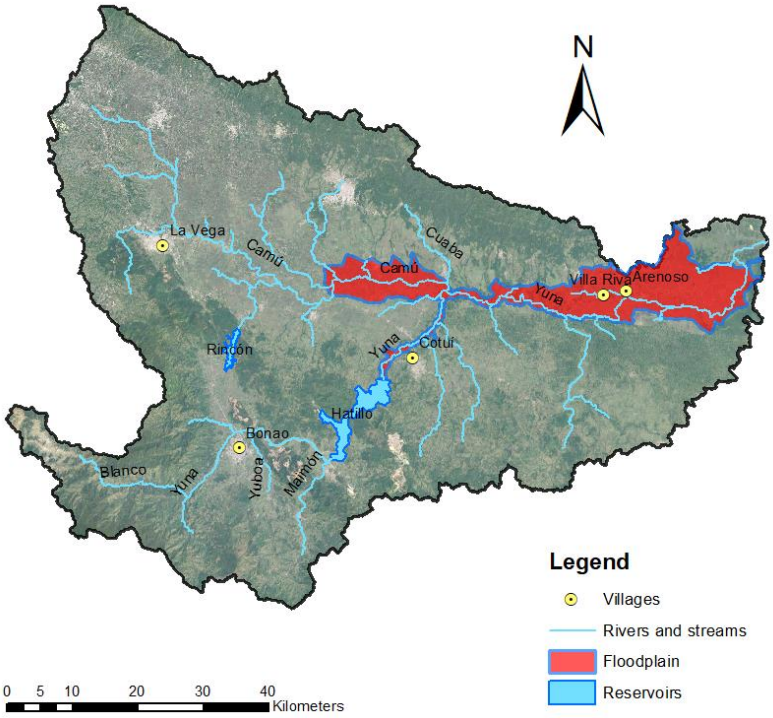

Figure 2. Floodplain in the lower Yuna basin.

At present, only 26 percent of the basin area is regulated by reservoirs. Hatillo is the most representative, regulating 23 percent of the total area of the basin (1,192 km^2). This reservoir is the largest body of surface water in the Dominican Republic, covering an average area of 27.4 km^2. The system has a dam built on a 50-meters-high embankment of earth and rock. The reservoir has a total storage capacity of 441 million cubic meters with a maximum length of 15 km. The minimum operating level is 70 meters above sea mean level (MAMSL). The elevation of the crest of the spillway is 86.5 MAMSL, which corresponds to the maximum operating level, while the extraordinary maximum level is 100.75 MAMSL. The main components of the dam are presented in Figure 3. The reservoir has an uncontrolled spillway (i.e., no gates, only free overflow) with a maximum capacity of 650 m^3/s; there are two hollow jet valves for the bottom outlet, with a maximum capacity of 82 m^3/s each. A powerhouse with a Francis turbine has an installed capacity of 8 MW and an annual energy generation of 40 GWh, the maximum flow capacity of the turbine is 30 m^3/s. Hatillo's installed capacity is low compared to other hydroelectric plants in the Dominican Republic. Examples of other plants include Tavera (96

MW), Valdesía (54 MW) and Aguacate (52 MW). Downstream of Hatillo, large areas of land are used for agriculture in the lower Yuna river basin, predominantly for rice cultivation, which is the main food crop in the Dominican Republic (Moquete, 2004). The reservoir supplies water for the irrigation of approximately 27,000 hectares of crops.

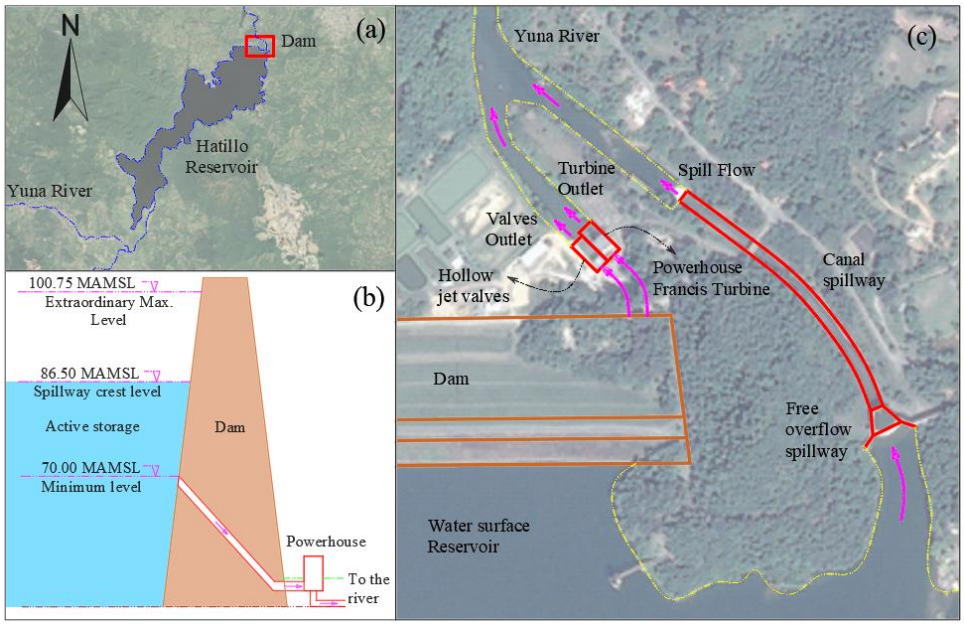

Figure 3. Dam components: (a) location of the dam, (b) operation levels, (c) schematic representation of the components of the dam.

The dam is operated by Empresa de Generación Hidroeléctrica Dominicana (EGEHID) and the Dominican Institute of Water Resources (INDRHI). The reservoir operation under normal conditions consists of discharging 26 m^3/s through the turbine throughout the day, then, this water returns to the Yuna river and it is used for irrigation. However, in emergency scenarios, such as in heavy rainy seasons or hurricane seasons, the National Dam Committee (COPRE) defines the actions for the operation of the reservoir. Releases through hollow jet valves occur when more water needs to be released due to flood control strategies or irrigation demands. Unfortunately, the information about operating rules of the reservoir were not available, as well as target levels, power production targets, and irrigation discharges. Nevertheless, daily data of inflows, spills, turbine discharges, valve outlets and total outflows, for the period 2009-2019 were provided by EGEHID, and from these data it was observed that 54% of the reservoir outlets are through spill, 45% are through the turbine and 1% are through the bottom valves. The fact that most of the reservoir releases have not been controlled (i.e., through spillway) allows us to hypothesize that the flood control objective can be improved.

It is important to mention that given the lack of reservoir operation rules, this study sought to emulate the real operation (2009 - 2019) using ML models, which is described in the next section. Additionally, due to the lack of target levels, power production targets, irrigation demands and specific objectives of the reservoir, an operation model has been proposed to be

optimized by applying three objectives with which it is sought to emulate the interests in the operation of the reservoir.

3 Machine Learning (ML) Models and Data

The reservoir operations in terms of daily release can be parameterized using mathematical functions adjusted to the patterns or shapes that define them. To this end, some artificial intelligence techniques or ML models, most notably ANNs, have proven to be efficient; some have even been classified as universal approximation functions (Tikk et al., 2003). Several authors have shown the benefits of these functions in the analysis of reservoir operation. Not only can they learn and replicate real operating behaviours (Ehsani et al., 2016; Zhang et al. 2018), they also adjust to artificial behaviors induced by purpose fulfilment in optimization problems (Momtahen & Dariane, 2007; Giuliani et al., 2016). The present study proposes two types of ANNs as approximation functions: the MLP and the RBN, in addition to a linear approximation function (LF).

MLP: Figure 4(a) shows the general scheme of an MLP. The information that enters the network is propagated forward using connections with different values or weights. The MLP has an input layer, where the data is entered, which is processed in the neurons of the hidden layers using activation functions until reaching the output layer, where the results are generated. The function that the MLP represents is as follows:

$$y_t = c + \sum_{i=1}^{N} v_i f_i(I_t \cdot w_i + b_i) \tag{1}$$

where N is the number of neurons with an activation function $f(\cdot)$ (e.g., sigmoidal function); I_t is the input vector of the network; w_i is the vector that represents the connections between the input and the hidden layer; v_i is the vector for the connections between the hidden layer and the output layer; b_i is the vector of bias for the neurons of the hidden layer and c is the bias of the output layer. The number of parameters in this network is $p = N(M + 2) + 1$, where M is the number of input variables for the model.

RBN: These networks use Gaussian functions for data processing, incorporating the center and radius parameters of processing units known as bases (instead of neurons, as in MLPs). Figure 4(b) shows the general schematic of an RBN. The function that the RBN represents is as follows:

$$g_i(I_t) = exp\left[-\sum_{j=1}^{M} \frac{\left[(I_t)_j - c_{j,i}\right]^2}{r_{j,i}^2}\right] \tag{2}$$

$$y_t = \sum_{i=1}^{N} w_i, g_i(I_t) \tag{3}$$

where, N is the number of bases with Gaussian functions g_i; w_i is the weight vector between the hidden layer and the output layer; I_t is the input vector of the network; M is the number of input variables and $c_{j,i}$ and $r_{j,i}$ are the center and radial vectors of each base with the dimension M. The number of parameters for an RBN is $N(2M + 1)$.

LF: These are the mathematical functions used to find relationships between variables with linear trends. Unlike the previous functions, they do not have the ability to accurately replicate complex patterns. If Y_t is a dependent variable and X_P the independent variables, the function can be expressed as follows:

$$Y_t = \beta_0 + \beta_1 X_1 + \beta_2 X_2 + \cdots + \beta_P X_P \tag{4}$$

where Y_t is the dependent variable; $X_1, X_1, \ldots X_P$ are the independent variables (input vector) and $\beta_0, \beta_1, \ldots \beta_P$ are the p parameters of the function.

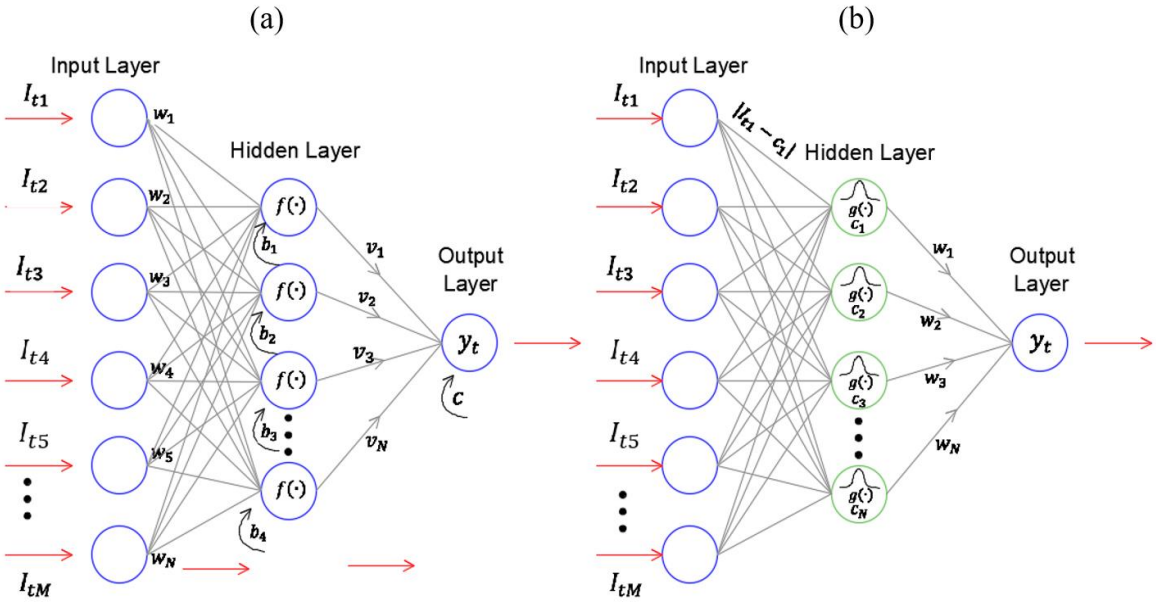

Figure 4. Architecture of the ANN: (a) MLP, (b) RBN.

The period of analysis for the case study was defined from the information available on the reservoir's operation; it corresponds to the period of 2009 to 2019, with daily time steps. These data consist of series of inflows, levels and outflows of the reservoir (Figure 5), in addition to storage elevation curve, area elevation curve and evaporation losses. A common practice carried out in artificial intelligence techniques is the normalization of data to improve the model (Emanueli Gandara, 2017). In this study, the data are standardized using the standard scoring method, which considers the variance and the mean of the time series as follows:

$$X_n = \frac{X - \mu}{\sigma} \tag{5}$$

where X is the value of the variable without standardization, μ is the average of the time series and σ is the value of the variance of the time series.

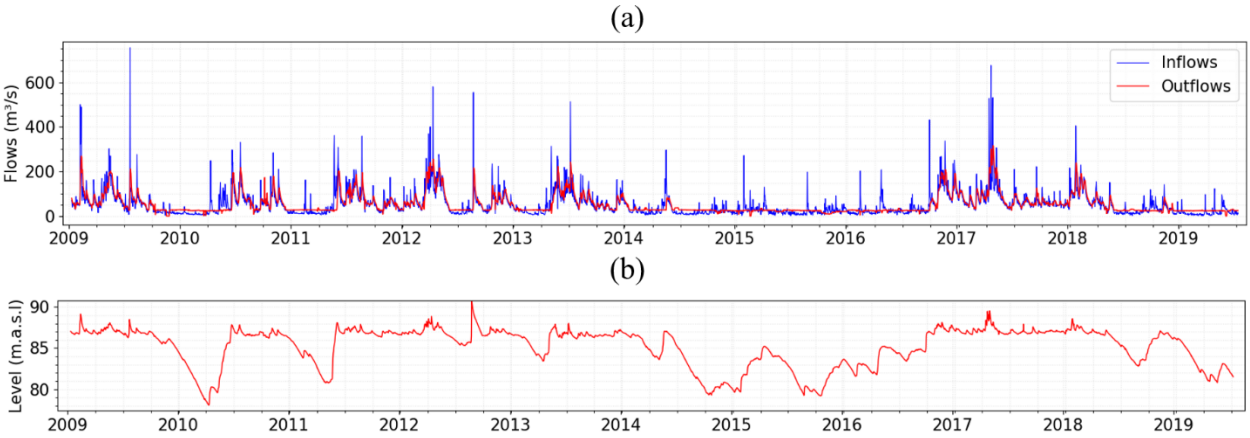

Figure 5. Data of the analysis period: (a) Inflows and outflows of the reservoir, (b) Levels of the reservoir.

4 Learning and Simulation of the Current Operation for the Reservoir

For the case study, as mentioned in section 2, there are no defined operating rules. Therefore, what is sought with the ML models is to simulate the operation of the reservoir. That is, to represent the amount of water that must be released at each time step through a ML model that learns to make decisions to meet certain objectives or goals. Initially, the parameterization of the reservoir's actual discharge R_t was sought for the analysis period, in which three ML models were tested: MLP, RBN and LF. The outputs R_t correspond to total discharges (i.e., turbine discharge, valves discharge and spills). Considering that correlation coefficient is commonly used to determine mathematical linear relations between two samples of random variables, or time series (Corzo, 2009), to select the input variables of the ML models, correlation analyses were performed between discharges at each time step t and the other time series (i.e., inflows, reservoir levels and previous discharges). Correlation analysis revealed that for the inflows q, the levels S and the previous discharges R, each using a lag times of 1 and 2 days (q_{t-1}, q_{t-2}; S_{t-1}, S_{t-2}; R_{t-1}, R_{t-2}) have the highest correlation values with respect to discharges R_t (Figure 6).

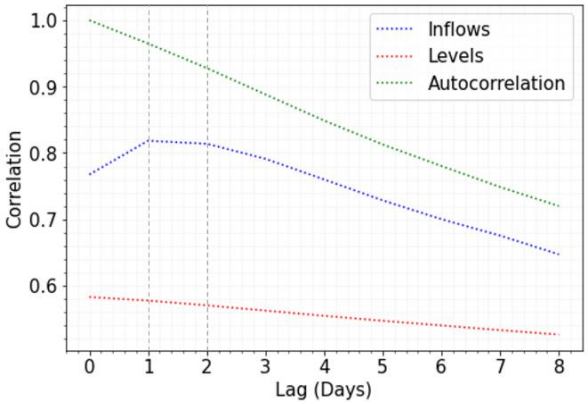

Figure 6. Correlation analyses for the selection of ML inputs: between inflows and discharges (blue); levels and discharges (red); and autocorrelation of discharges (green).

Using these six inputs for all ML models, different configurations for MLP and RBF were tested varying the number of Neurons (MLP) or Basis (RBF). The results revealed that a 6-7-1 MLP configuration (i.e., 6 inputs, 7 neurons in a hidden layer and 1 output layer), with the application of a sigmoid activation function (Equation 6, which variables are same as for Equation 1), generated the best results (MSE 26.75 and MAE 2.97). The Scikit-learn Python library (Pedregosa et al., 2011) was used for MLP and LF models, while for RBN, Keras was used (Chollet, 2015). In all ML models, 80 percent of the data was used for training and 20 percent for the test. In the case of MLP, configurations with several layers and different numbers of Neurons (Deep Learning) were tested, however, in this case, by increasing the complexity of the network with more hidden layers and Neurons, the results are not improved but the number of parameters and decision variables (weights and biases) is increased. Therefore, simple configurations of a single hidden layer and a maximum of 7 Neurons in the hidden layer were chosen.

$$f_i = \frac{1}{(1 + e^{-(I_t \cdot w_i + b_i)})} \tag{6}$$

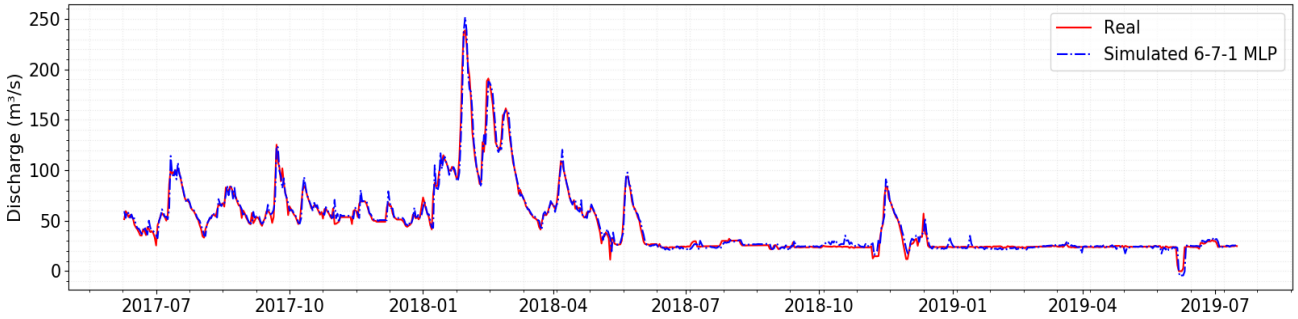

Figure 7. Test Results for 6-7-1 MLP configuration.

Table 1. Test Results for ML models

Measures	MLP			RBN			LF	Naïve
	6-7-1	6-6-1	6-4-1	6-7-1	6-6-1	6-4-1		
MSE	26.75	28.46	27.59	26.90	29.93	29.99	38.74	47.54
MAE	2.97	3.27	3.14	2.92	3.32	3.20	3.60	3.38
Correlation	0.988	0.987	0.988	0.988	0.987	0.987	0.982	0.978
Nash-Nutcliffe	0.976	0.974	0.975	0.976	0.973	0.973	0.965	0.957

Table 1 shows the test results for each of the ML models, and are compared against a neutral model such as the inertia forecast or Naïve forecast. Note that the best results are obtained for the MLP and RBN models in all the performance measures used, mainly for the MSE, which is an indicator that penalizes large errors. However, for the other measures, there are no very large differences with respect to the LF and Naïve models. This could be due to the inertia of the system, that is, for the actual operating condition of the reservoir, the daily discharges do not

vary considerably from one day to the next. For example, when there are no spillway discharges, the daily outflows under normal conditions are 26 m^3/s as mentioned in chapter 2 and as shown in Figure 7 between June 2018 and July 2019. This means that the actual operation of the reservoir for that period can be very predictive for any model.

5 Reservoir operation Model

A reservoir operation model was built from the data from the period of analysis. This model integrates water balances, physical constraints of the dam components and the ML models, the latter defining daily controlled discharges. The water balances determine the volume of the reservoir at each time step *t*, the level and the surface area are calculated by applying the storage-elevation curve and the area-elevation curve respectively. The water balance equation is as follows:

$$V_{t+1} = V_t + V_{et} - V_{spill} + V_{sc} - EVP \tag{7}$$

where V_{t+1} (subject to $V_t \geq 0$) and V_t correspond, respectively, to the storage volume of the reservoir for the next time step $(t + 1)$ and the present time step t; V_{et} corresponds to the input volumes of the reservoir for the present time step t, taking the input discharge time series; EVP corresponds to the evaporation loses, which are calculated based on the surface area of the reservoir and the month of the year; V_{spill} corresponds to the spilled volume of the reservoir for the present time step t, which is calculated as a function of the height above the crest of the spillway and V_{sc} corresponds to the controlled outlet volume of the reservoir and is defined from the ML models.

The three ML models of MLP, RBN and LF are defined, each using the same inputs, from those used to learn the current reservoir operation (see section 4). The outputs of the models correspond to the reservoir's controlled discharges Q_{sc} for each time step.

$$Q_{sc} = f(I_t) \tag{8}$$

$$Q_{sc} = f(q_{t-2},\ q_{t-1},\ S_{t-2},\ S_{t-1},\ R_{t-2},\ R_{t-1}) \tag{9}$$

MLP: Three configurations are proposed. The first is equivalent to the best that was obtained to simulate the current reservoir operation (6-7-1). The second is an MLP with six neurons (6-6-1), and the third is an MLP with four neurons (6-4-1). A sigmoid function is used as the activation function, which corresponds to Equation 6. The initial MLP parameters are generated randomly for the domain $-1 \leq w_i, b_i, v_i, c \leq 1$.

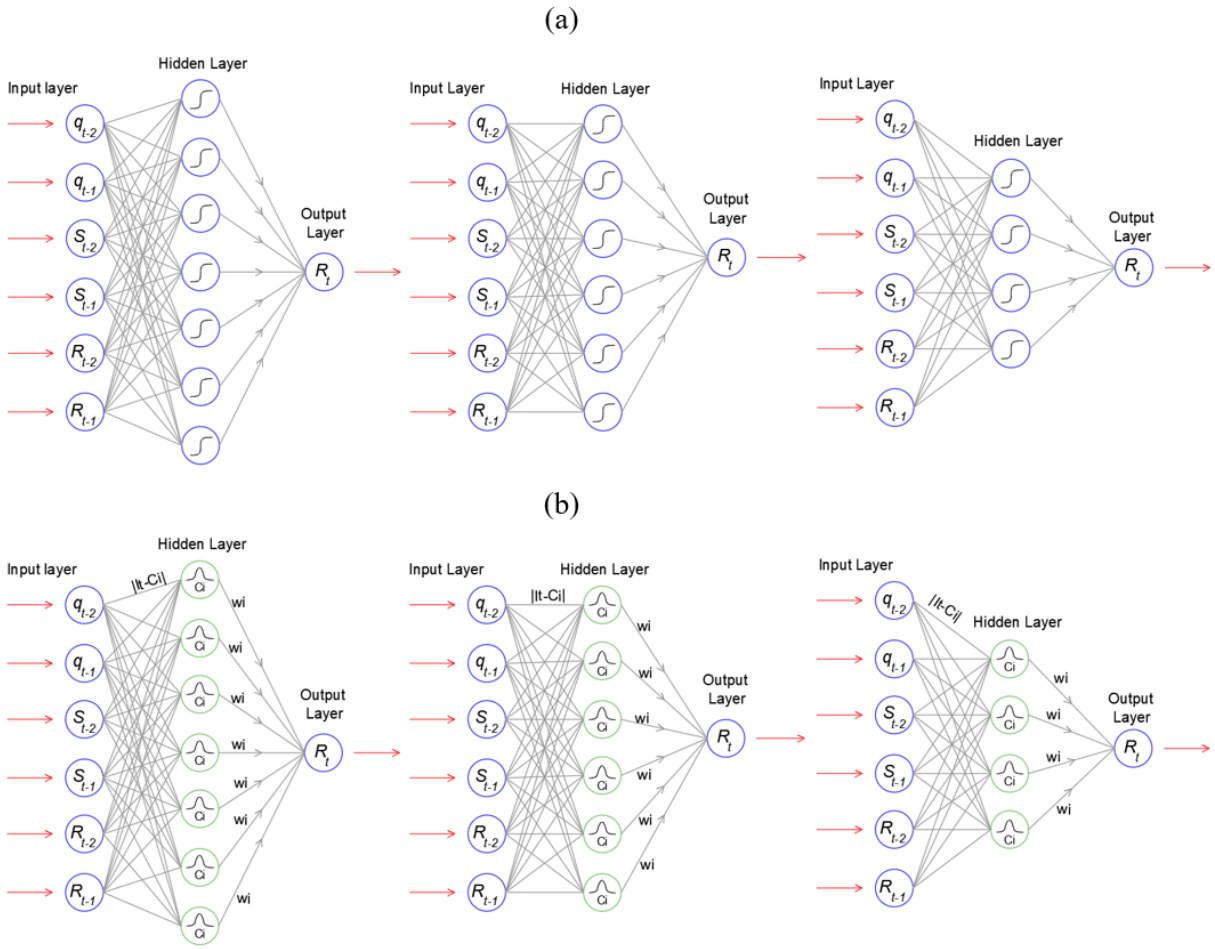

Figure 8. Configuration of the (a) ANN and (b) RBN proposed for the operation models.

RBN: Like the MLPs, 6-7-1, 6-6-1 and 6-4-1 configurations are proposed. Figure 8(b) illustrates these three networks. The initial parameters of the RBNs, like the MLPs, are generated randomly for the domain $-10 \leq c_i, r_i, w_i \leq 10$.

LF: The linear function is proposed to evaluate linear patterns in the behavior of the reservoir operations, and to compare against the other proposed functions. The parameters of the LF, like those of the previous functions, are initially generated randomly for the domain $-5 \leq \beta_0, \beta_1, \beta_2, \beta_3, \beta_4, \beta_5, \beta_6 \leq 5$.

Each of the ML models are coupled to the reservoir operation model to define the controlled discharges at each time step *t*. The physical constraints of the dam components are also incorporated. These defines turbine capacities, exhaust capacities, discharge limits, and minimum and maximum operating levels. In summary, a reservoir operation model is built in which seven different ML model configurations are tested, each one elaborated in Python. The parameters of the ML models are the decision variables of the optimization process, described later.

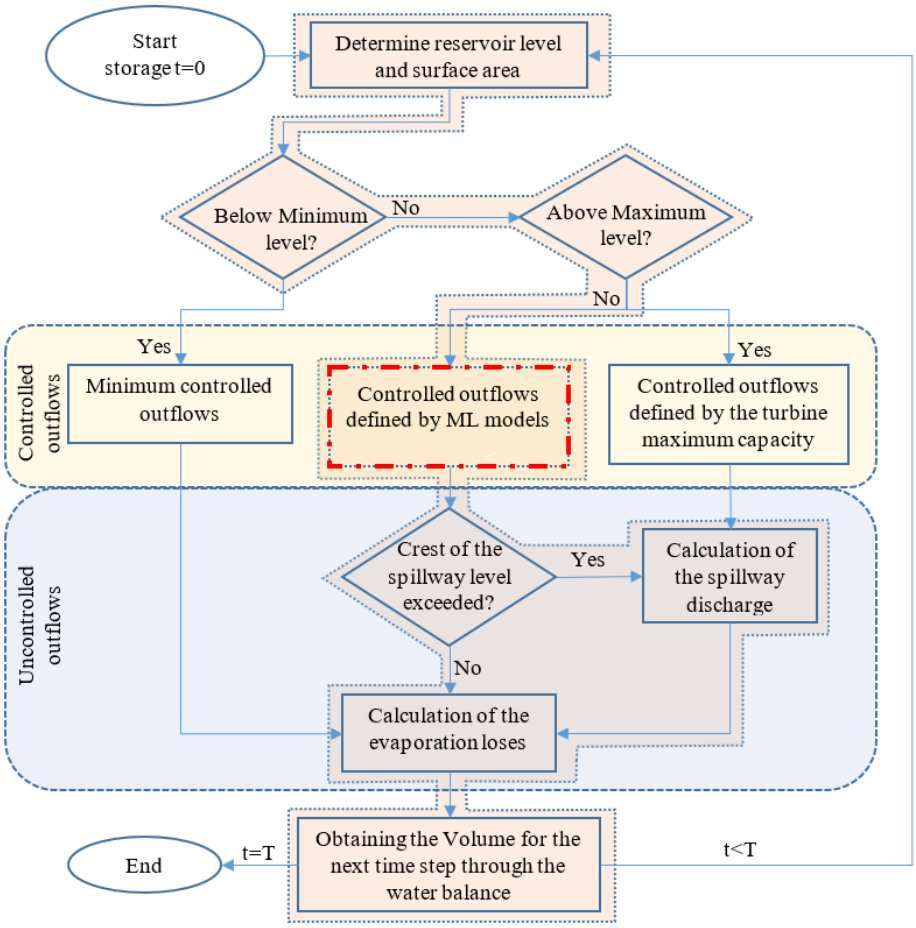

Figure 9. Flow diagram of the reservoir operation model built for the Hatillo reservoir.

Figure 9 summarizes the step by step of the reservoir operation model. Starting with the storage volume of the first day of analysis, reservoir level and surface areas are determined applying the storage-elevation curve and the area-elevation curve.

The outflows of the reservoir can be controlled through the Francis turbine and the two hollow jet valves. The controlled discharges of the reservoir are defined by the ML models taking into account the respective capacity constraints (Equation 10 and 11). Therefore, conditional rules are used to limit minimum and maximum controlled outflows.

Limits of the reservoir levels are proposed. A minimum level (75 m.a.s.l) is considered to guarantee that when there are low levels during dry periods, the turbine discharges a minimum flow during the day. Unfortunately, there is no information available on critical flow thresholds, below which significant environmental impacts occur. Berge et al. (2003) proposed downstream of the dam a minimum flow of 3 m^3/s to have the necessary recipient capacity for pollutants, and to support aquatic life. However, in this study the minimum flow is assumed based on the historical data of outflows from the reservoir taking the flow that is statistically exceeded 95% of the time (7.5 m^3/s).

On the other hand, a maximum level value (87.5 m.a.s.l) is proposed from which the maximum flow capacity of the turbine can be released. So then:

$$Q_{sc} = \begin{cases} Q_{sc\_min} & if\ S_t < S_{min} \\ Q_{turb\_max} & if\ S_t > S_{max} \\ Q_{ML} & if\ S_{min} < S_t < S_{max} \end{cases} \quad (10)$$

$$Q_{sc} = Q_{turb} + Q_{valv} \quad (11)$$

Where S_t is reservoir level at time t; S_{min} is the proposed minimum threshold level; S_{max} is the proposed maximum threshold level; Q_{sc_min} is the minimum discharge (7.5 m^3/s); Q_{turb_max} is the maximum discharge through the turbine (30 m^3/s); Q_{sc} are the controlled discharges of the reservoir at t; Q_{ML} are the discharges obtained with the ML model. Q_{turb} are the turbine discharges at t subject to $7.5\ m^3/s < Q_{turb} < 30\ m^3/s$. Q_{valv} are the hollow jet valves discharges at t subject to $0\ m^3/s < Q_{valv} < 164\ m^3/s$.

Once the controlled discharges have been defined, reservoir level is verified with respect to spillway crest level, if this is exceeded, the spillway release is calculated as a function of the height above the crest of the spillway. The specific rating curve of the spillway for Hatillo reservoir is available at Viparelli (1983). After all outflows (i.e., controlled and un-controlled) are defined, including the evaporation losses, reservoir volume for the next time step is obtained by means of water balance, starting the process again and so the cycle continues until the analysis period is completed. The route shaded in orange in the flow diagram (Figure 9) corresponds to the main operating route in this proposed model (i.e., when the levels are within the defined threshold), where the segmented red rectangle highlights the component of ML models.

6 Optimization

The optimization process uses the **reservoir operation model** to identify what parameters of the ML models represent the best solutions (i.e., non-dominated solutions). There are three objectives: to control flooding, to supply water for irrigation and to generate hydroelectricity.

OF1. Flood control: The goal is to minimize excess flow Q_t^{flo} in each time step t from the reservoir's daily discharge q_t^R (m^3/s) with respect to a proposed limit flood flow $\overline{q}$. The following function defines OF1 for the entire analysis period T:

$$OF1 = \sum_{t=0}^{T} (Q_t^{flo}) \quad (12)$$

$$Q_t^{flo} = \begin{cases} 0 & if\ q_t^R \leq \overline{q} \\ (q_t^R - \overline{q})^2 & other\ wise \end{cases} \quad (13)$$

In the present study, a flow limit is proposed from which the optimizer seeks to punish the discharges. Similarly to Saavedra et al., (2010), this limit flow is set as the average of all the daily discharge values (Q_i) of the reservoir that exceeded the average discharge flow of the series (Q_{mean}). Therefore, using equation 14 the flow limit $\overline{q}$ is obtained, where n = number of records.

$$\overline{q} = \sum_{i=1}^{N} \frac{Q_i}{n}; \quad Q_i > Q_{mean} \tag{14}$$

OF2. Water supply for irrigation: The goal is to minimize deficits in the irrigation water supply Q_t^{irr} in each time step t from the reservoir's daily discharge q_t^R (m^3/s) with respect to the water demand for irrigation d_t. The following function defines the OF2 for the entire period of analysis T:

$$OF2 = \sum_{t=0}^{T} \left(Q_t^{irr}\right) \tag{15}$$

$$Q_t^{irr} = \begin{cases} 0 & if\ q_t^R > d_t \\ (d_t - q_t^R)^2 & other\ wise \end{cases} \tag{16}$$

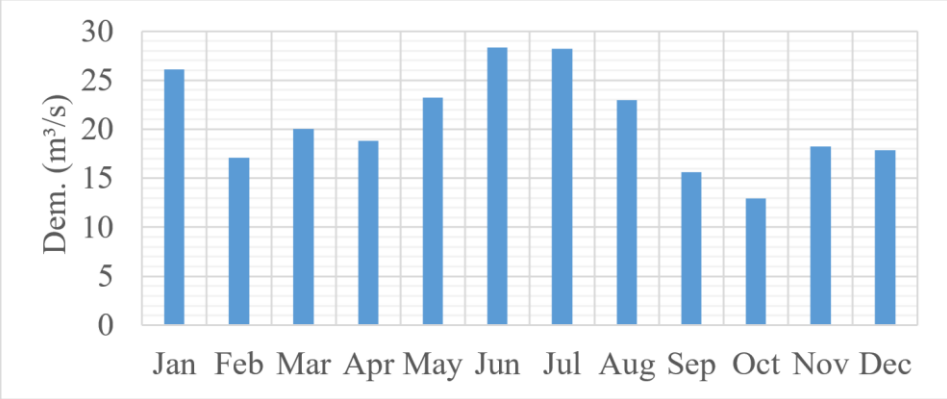

Figure 10. Demand for irrigation downstream of the reservoir.

Irrigation demands were obtained using the CROPWAT program (Smith, 1992). Taking into account that the cultivation of rice demands the greatest amount of water and covers the largest area of crops in the lower Yuna, irrigation demand calculations were made from the requirements and the cycle of the rice cultivation. Rice in the Dominican Republic has two sowing periods in the year, the first, from December to April, and the second, covers the months of June, July and August (Moquete, 2004). Climatic data (Temperature, Humidity, Wind speed, hours of sunshine), and rainfall data were provided by INDRHI (taking monthly mean data for the analysis period). From the cultivation areas, the monthly average demands for the analysis period (2009-2019) were calculated, which are shown in Figure 10.

OF3. Hydropower generation (Total): The goal is to maximize the power generated (KW) for the entire analysis period T from the powers generated in each time step P_t. The following function defines the OF3:

$$OF3 = \sum_{t=0}^{T} P_t \tag{17}$$

$$P_t = \eta\, \gamma H_t q_t^{turb} \tag{18}$$

$$\eta = f\left(q_t^{turb}\right) \tag{19}$$

where γ is the specific weight of water; H_t is the hydraulic head, which depends on the reservoir's water level and the elevation of the turbine axis; η is the efficiency of the turbine as a function of the discharge; and q_t^{turb} is the discharge through turbine (m^3/s). It is important to mention that a conversion factor of -1 is applied to the OF3 (equation 17) within the optimizer in this study, since the modules used by the program (JMETALPY) work only for minimization objectives (Benítez-Hidalgo et al., 2019).

In hydroelectric plants, there are other important indicators such as firm energy, with which the energy security of a system can be evaluated. Due to the fact that Hatillo hydroelectric plant has a low installed capacity compared to the large hydroelectric plants in the Dominican Republic, total energy is the only objective considered in this study. This simplifies the optimization process; however, a firm energy indicator is evaluated in the results obtained (chapter 8).

7 Computational Experiments

Optimization was performed using the analysis period (2009-2019). Two EAs were used to optimize the operation model: the NSGAII and the MOEA / D. JMETALPY (Benítez-Hidalgo et al., 2019), a multi-objective optimization environment (developed in Python) that contains a set of modules with different multi-objective and single-objective optimization algorithms, was also used. With JMETALPY, a set of problems were used to evaluate the optimization algorithms. The operation model was inserted into JMETALPY as a subclass of floating problems. The values for population size and individual parameters in the algorithms largely depended on the optimization problem (Ritter, 2016). Trial and error tests were carried out using various population ranges to select the population size; populations greater than 100 individuals did not improve the results and increased the computational time needed for the NSGA II. For the MOEA / D, the population was defined as 300 individuals. For the other parameters, trial and error tests were performed using small populations (up to 50 individuals) so that the program could converge rapidly. Default values were taken as a basis for the algorithms.

The optimization process was developed by a computer with 16 GB of RAM and eight 2.6 GHz cores. The codes were executed by implementing the MultiprocessEvaluator module, which allowed faster calculations and for different individuals within the same generation to be calculated in parallel. On average, the program reported convergence for each operating model after eight hours in 10,000 evaluation processes.

Using the JMETALPY display module, the Pareto fronts were obtained for each of the program executions. For each model, a 3D Pareto front was generated, having been optimized by both the NSGAII algorithm and the MOEA / D. A total of 14 models were simulated. As mentioned above, the decision variables were the parameters of the ML models. Therefore, the optimized parameters for MLP were weights and biases; In RBN models they were centers, radii and weights; and for LF the coefficients. The parameters are summarized in table 2.

Table 2. Parameters of the optimization process.

	MLP			RBN			FL
Parameters	6-7-1	6-6-1	6-4-1	6-7-1	6-6-1	6-4-1	
Weights (w_i, v_i)	42+7	36+6	24+4	7	6	4	-
Bias (b_i)	7+1	6+1	4+1	-	-	-	-
Radius ($r_{j,i}$)	-	-	-	42	36	24	-
Centers ($c_{j,i}$)	-	-	-	42	36	24	-
LF Coef.	-	-	-	-	-	-	7
Total	57	49	33	91	78	52	7

8 Results

After compiling the Pareto fronts generated by the optimizers, non-dominated solutions were obtained. These represent different reservoir operations in terms of daily releases. Figure 11 shows the 3D Pareto front that compiles all the optimal solutions from the reservoir operation model. Each graph point corresponds to a different reservoir operation obtained by the optimizers. The solutions constructed by the MLP are the closest to the ideal optimum solution (black point). The real reservoir operation from the analysis period is represented by the yellow point; the rectangles shaded in red represent decisions space regarding reservoir operations that equaled or improved the real operation per the three objectives. For the objective function OF3 (a maximization function), a minimization function with a conversion factor of -1 was used; since the modules used by JMETALPY in the present study work only for minimization objectives.

Figure 12 shows the envelope of hydrographs generated by simulating all the obtained reservoir operations reflected in Figure 11. The envelope of levels is presented in the same way. The mean values of the reservoir operations for the entire population are shown in dark blue, and the gradient color shows the quintiles. The red line represents the real operation of the system; here, the peaks of the hydrographs approach the maximum values of the envelope, maintaining high operation levels compared to the mean of the optimized reservoir operations. This could be due to the fact that the current operation gives more priority to OF2 and OF3, which may be more associated with high levels of the reservoir. Note that in dry periods such as the one between the middle of 2014 and the end of 2016, most of the solutions obtained were close at certain times to the minimum level defined for the reservoir (75 m.a.s.l). This can be understood as the consequence of water discharges to meet irrigation demands (OF2), in addition to having more capacity to buffer the volumes of the following wet season (OF1). In this study, the analysis period was evaluated globally, without distinguishing between dry and wet periods. Therefore, optimizers look for the best solutions by taking stock of the entire analysis period. Future works could incorporate different operations for the reservoir depending on the seasons of the analysis period.

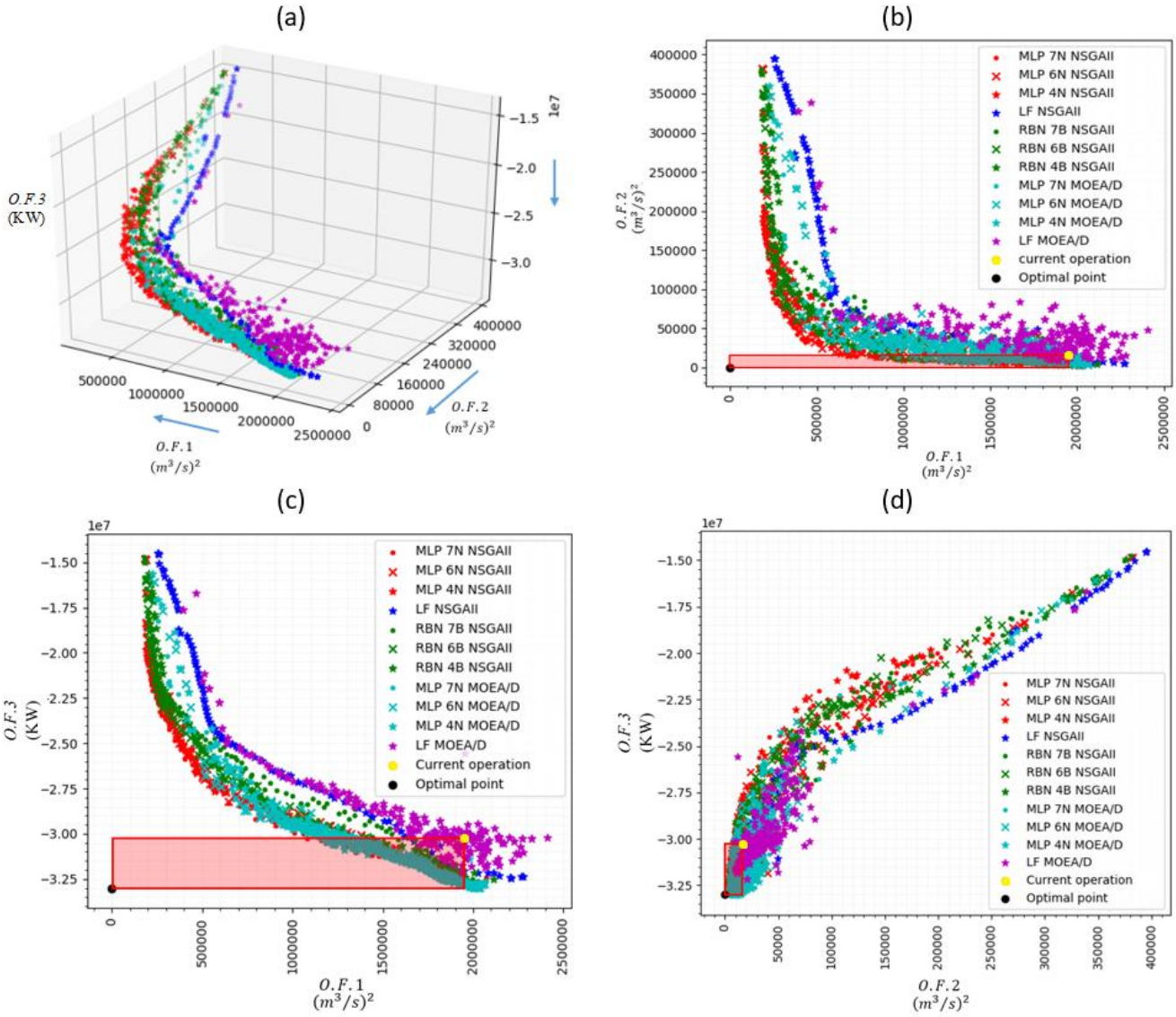

Figure 11. Unified Pareto fronts. (a) all the operation models; (b) operation models OF1–OF2; (c) operation models OF1–OF3; (d) operation models OF2–OF3.

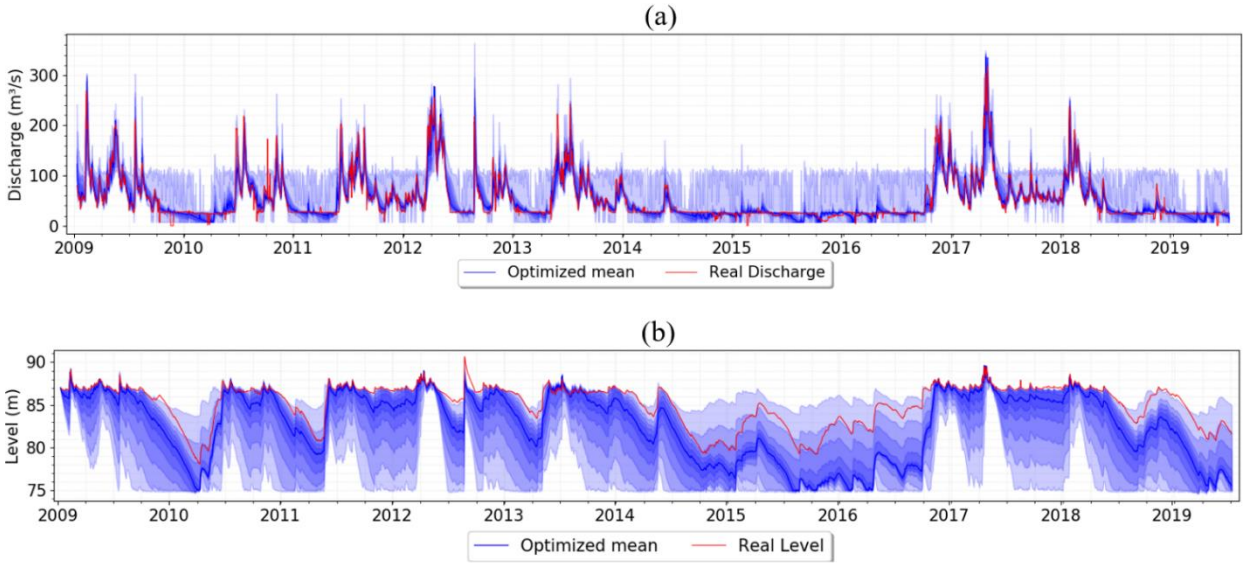

Figure 12. Envelope for hydrographs generated by all reservoir operations obtained from optimization. (a) flow rates and (b) levels. The mean values of the reservoir operations for the entire population are shown in dark blue, and the gradient color shows the quintiles.

Figure 13 shows the comparative values (Parallel graphic) of the different solutions for each of the three objectives. Additionally, the maximum peak flow and a firm energy indicator generated by each reservoir operation for the entire time series have been added. The firm energy $(F.E)$ is evaluated considering the daily power that can statistically be exceeded 95% of the time, or in other words, the 5th percentile of all daily power generation: $F.E = PCTL_5(P_{t,1}, P_{t,2}, \dots, P_{t,T})$. The segmented black line reflects the evaluation of the three objectives plus firm energy and peak flow for the actual operation of the reservoir in the analysis period. As shown in the hydrograph and level envelope (Figure 12), and it is also reflected in figure 13, the current reservoir operation aims to meet the objectives OF2 and OF3 (i.e., water for irrigation and hydroelectric generation), but leaves considerable room for improvement in flood control OF1. Note that the firm energy is greater as the generated power increases (OF3), presenting correlation, however, certain reservoir operations are observed that considerably reduce the firm energy, this can be associated with the fact that these solutions generate minimal discharges when there are low levels in the reservoir at certain times (dry periods).

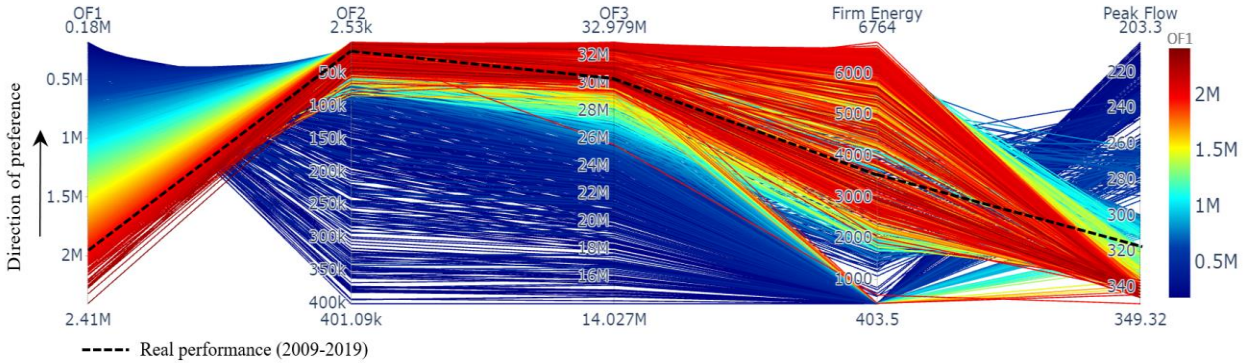

Figure 13. Comparison of results of all the solutions to reservoir operations for the three objectives, firm energy and peak flow.

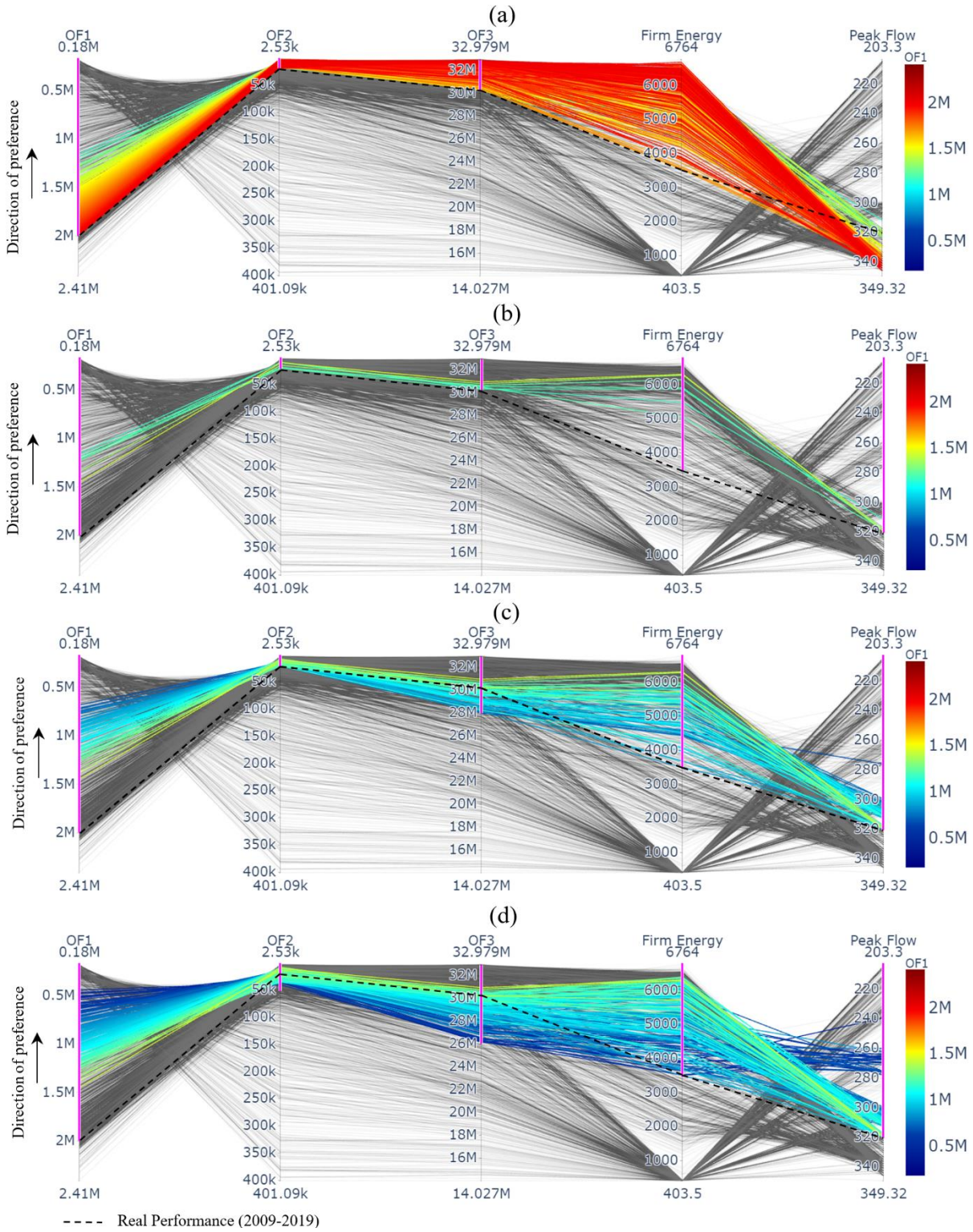

Figure 14. Parallel graphic. (a) Reservoir operations that improve the three objectives proposed for the current operation. (b) Reservoir operations that improve the three objectives, firm energy and peak flow for the current operation. (c) Reservoir operations that improve OF1 by reducing hydropower production. (d) Reservoir operations that improve OF1 by affecting both irrigation and hydropower production.

Figure 14 shows different groups of solutions: Figure 14(a) represents all the reservoir operations that equal or improve each of the three proposed objectives with respect to the current reservoir operation. As can be seen, these solutions also improve firm energy, however, some present peak flows above the peak of the current operation. Therefore, figure 14(b) illustrates the reservoir operations that improve the three objectives, firm energy and peak flows.

Given that for the current reservoir operation, flood control is the objective that has the greatest margin for improvement, as can be seen in figure 13, in another group of solutions, it is observed that by reducing hydropower production, greater benefits are obtained for the OF1. Figure 14(c) shows reservoir operations where energy production is decreased by 2 million KW. Note that this decrease allows for considerable improvements in flood control without affecting firm power and irrigation. Finally, for another group of solutions, it is observed that by affecting both irrigation and hydropower production, even better operations are obtained for flood control without affecting firm energy as can be seen in figure 14(d). The above, increasing the OF2 to 50,000 $(m^3/s)^2$ and reducing the OF3 to 26 million KW.

Table 3. Hypervolume indicator for optimized models

Operation Model		Hypervolume (10^{19}) NSGAII	MOEA/D
Lineal Function		1.06	1.03
MLP	4N	1.33	1.26
	6N	1.31	1.26
	7N	**1.34**	1.26
RBN	4B	1.26	-
	6B	1.27	-
	7B	1.19	-

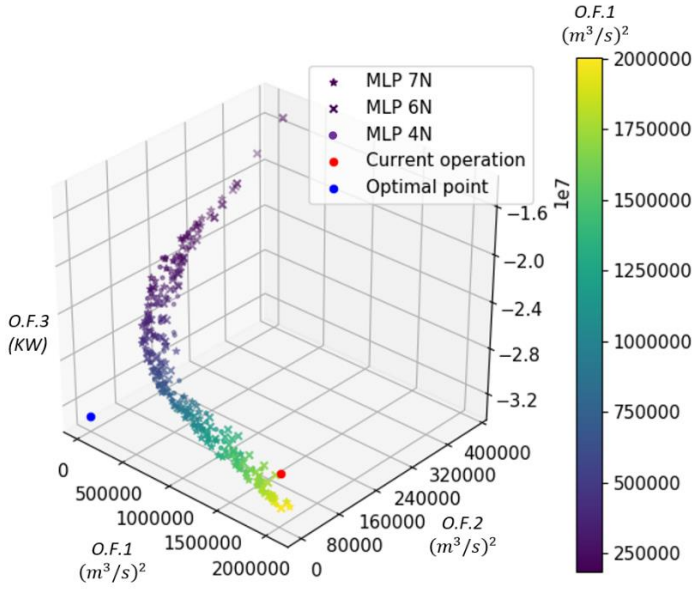

Figure 15. Pareto front for models with MLP and NSGAII optimizers.

Based on the hypervolume indicator and the compiled Pareto fronts (Figure 11), the ANN models offer the best results overall. It is evident that the MLP models tend to generate the best results for this case study. This may be due to the fact that RBN models use a greater number of parameters (decision variables), which implies greater difficulty for optimization. The results were similar regardless of the settings used for each ML model. The 6-7-1 MLP configuration had the best results overall, being better when using the NSGAII algorithm. For the RBN, the 6-6-1 configuration (using the same algorithm) yielded the best results. When comparing the two optimizers, similar results were observed between the MLP functions, with better outcomes from the NSGAII. This may be because the decision space in this study was not oriented towards a specific area of preference; however, the MOEA / D results may be improved by narrowing the decision space (Ma et al., 2015). Biasing the Pareto Front towards a specific area, better convergence could be achieved by covering an area of interest. Regarding the RBN functions, the MOEA / D optimizer did not converge. In the case of the LF, the results were considerably lower according to the hypervolume indicator, which shows that this function does not simulate reservoir operations in the best way.

Some of the solutions obtained for the reservoir operations are selected and simulated in order to evaluate their performance. Figure 16 shows in detail the Pareto front OF1–OF2 and OF1–OF3, where red shaded rectangles indicate the decision space of the solutions that equal or exceed the reservoir's actual operations towards the three objectives. Some points located inside and outside the decision space are simulated and compared with the real operation: four reservoir operations shown in figure 14(b) are simulated (MLP_7N_23; MLP_7N_37; MLP_7N_41; MLP_7N_72), as well as two solutions shown in figure 14(c) (MLP_7N_40; MLP_7N_43) and two shown in figure 14(d) (MLP_7N_40; MLP_7N_43). Figure 16 (c) shows the selected solutions.

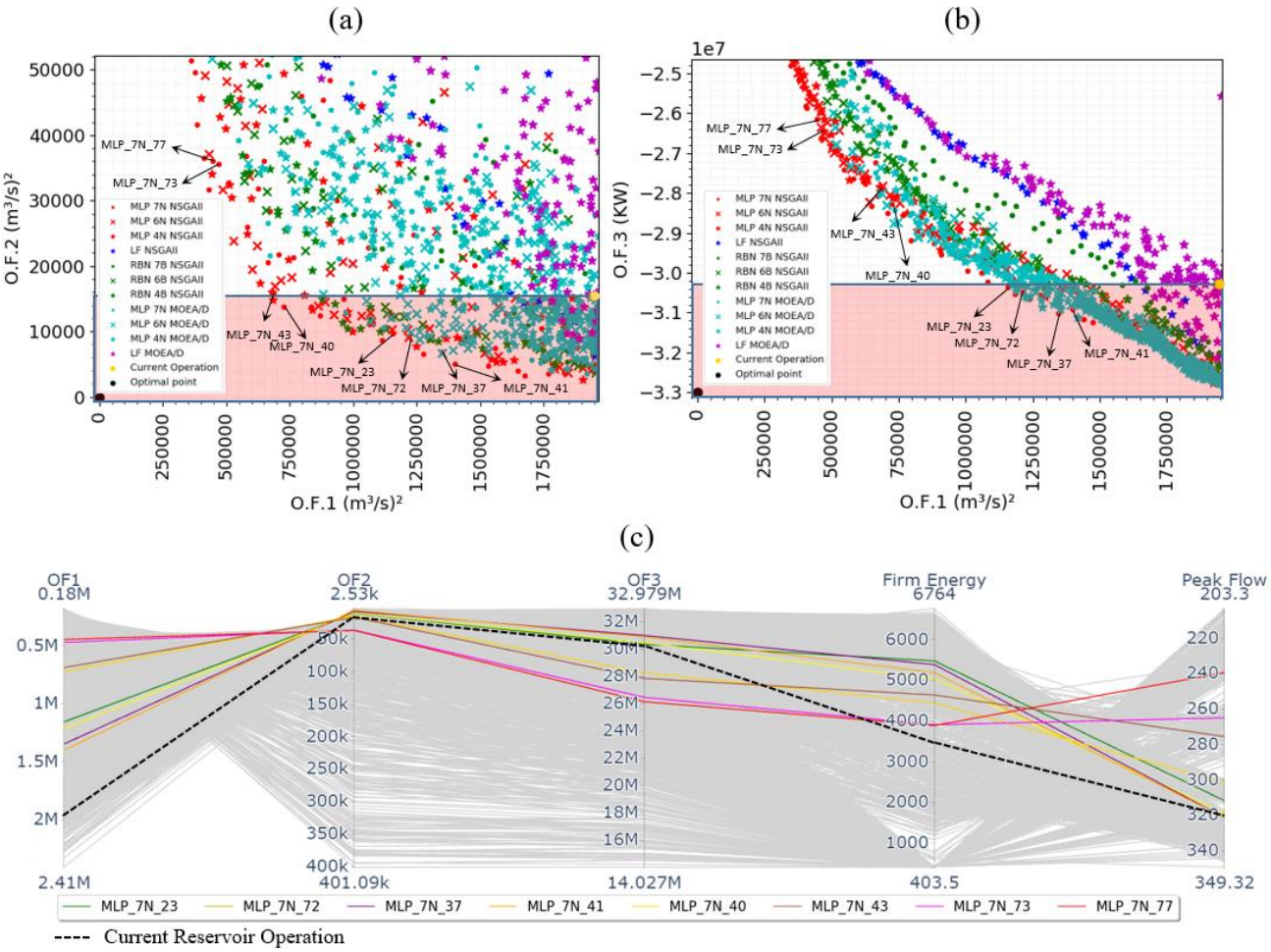

Figure 16. Zoomed-in Pareto front: (a) OF1–OF2; (b) OF1–OF3; (c) Parallel graphic of the selected solutions

Results are shown in Figure 17, which confirms that it is possible to reduce the peaks of the hydrograph of the current operation, as they are more to the left in the Pareto front. The MLP_7N_77 reservoir operation, as expected, had the best result in reducing all the peaks of the reference hydrograph (current operation), followed by MLP_7N_73. However, the effect negatively affected irrigation and power generation, keeping firm energy. Reservoir operations such as MLP_7N_40 and RN_7N_43, located within the shaded rectangle for the OF1 and OF2 (figure 16) allow to reduce peak flows by slightly affecting the total power (OF3) but improving the irrigation objective and keeping the firm energy. And finally, the MLP_7N_23, MLP_7N_37, MLP_7N_41, MLP_7N_72 solutions, located within the shaded rectangle for the three objectives despite not having the same peak flow reduction capacity as the previous ones, managed to reduce the reference hydrograph while increasing power generation and guaranteeing the supply of water for irrigation. Figure 18 shows the hydrographs of the reservoir operations selected for the wettest portion of the analysis period, which spanned from November 2016 to May 2017.

Note that all the selected operations improve the current operation in terms of flood control and firm energy, however, as expected, the operations with the best performance in flood control (i.e., MLP_7N_77 and MLP_7N_73) present some intermittence (i.e., presence of minimum values) in power generation and irrigation in dry periods, as can be seen in Figure 17, for example, in the months of February to March 2010 and in the months of July to September 2014. The MLP_7N_40 and MLP_7N_43 solutions present less intermittence than the previous solutions in these terms, even improving the irrigation objective and having a considerable improvement in flood control (see Figure 18). Regarding the solutions located within the red rectangles both in Figure 16 (a) and Figure 16 (b), they considerably improved the current operation in terms of intermittence in power generation and irrigation, and also improving the flood control objective (although not in the same magnitude as the previous solutions: MLP_7N_40 and MLP_7N_43).

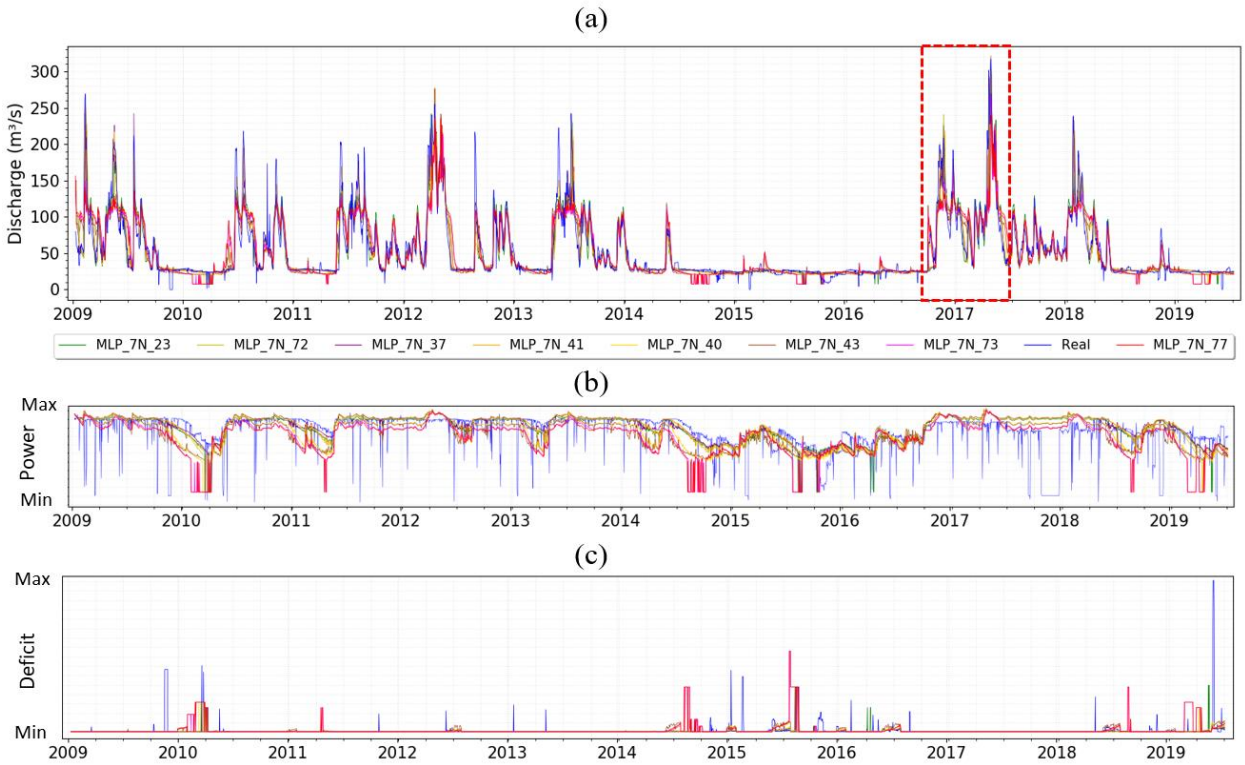

Figure 17. Simulation of the selected reservoir operations for the analysis period (2009–2019). (a) hydrographs of output flow; (b) generated power; (c) deficit in irrigation water supply.

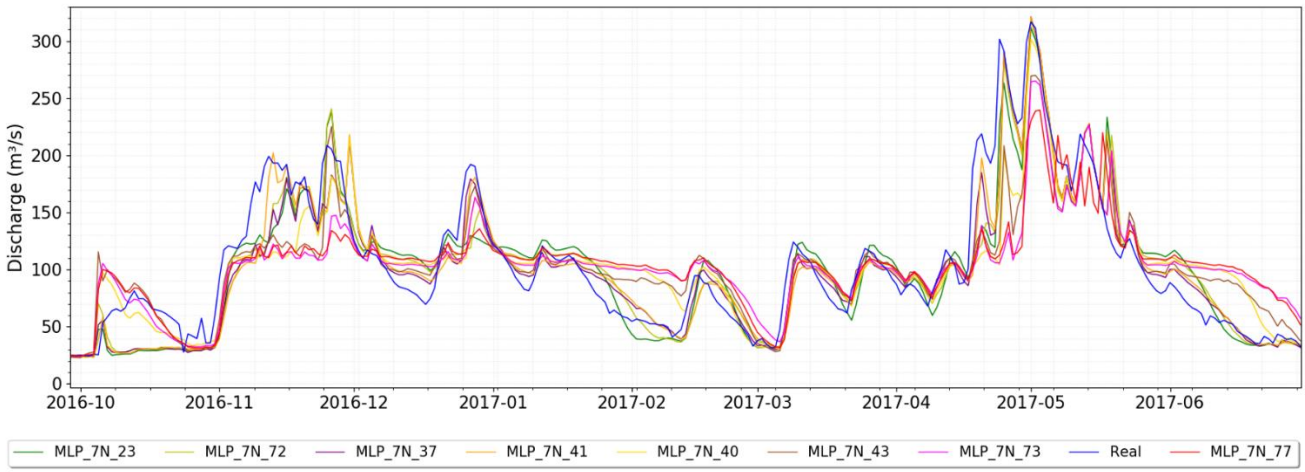

Figure 18. Hydrograph of the selected reservoir operations for the wet period (2016–2018).

9 Conclusions

This study compiled some artificial intelligence techniques and EAs to offer a methodology for obtaining optimal operations for multipurpose reservoirs. The approach was applied to a case study on the Hatillo reservoir in the Dominican Republic, which has three purposes: hydroelectric generation, irrigation and flood control. Through this study, reservoir operations were obtained that improved the current operation of the reservoir for each of the three proposed objectives. Through the Pareto fronts obtained, the wide variety of operations for the Hatillo reservoir can be evidenced, which could even serve as a reference for decision-making towards a balance of interests, thus improving the integral use of the reservoir.

Notably, the flood control objective of the reservoir's current operation was found to have wide room for improvement. Several reservoir operations were obtained that reduced the discharge peaks of the reservoir (as evidenced in the wet period from November 2016 to May 2017), equaling or even improving the objectives for irrigation and hydroelectric generation with respect to the current operation (e.g., MLP_7N_23; MLP_7N_37; MLP_7N_41; MLP_7N_72). Other reservoir operations, such as MLP_7N_77, considerably reduced the discharge peaks of the dam and only slightly affected the other purposes.

Overall, these results demonstrate that reservoir operation can be parameterized using ML models such as ANNs, which can accurately replicate the patterns and policies that govern reservoir operation. The 6-7-1 MLP configuration using the NSGAII optimizer had the best results overall. The MLP models tend to generate the best results for this case study. This may be due to the fact that RBN models use a greater number of parameters, making the optimization process more difficult. Results were similar regardless of the settings used for each ML model (i.e., varying the number of neurons). When the two optimizers were compared, similar results were observed for the MLP functions, with the NSGAII results being better. This may be because of the decision space in the present study was not oriented towards a specific area of preference; however, the MOEA / D results could be improved by narrowing the decision space (Ma et al., 2015). In the case of the LF, the results were considerably lower according to the hypervolume indicator, which showed that the reservoir operations did not adequately adjust to linear patterns.

The lack of information was one of the main limitations for the development of this research, although it was possible to have data from the reservoir for the period 2009-2019. For models based on data, such as those of the present study, it is desirable to have with longer time series. Unfortunately, the reservoir operation rules as well as target levels, power production targets, and irrigation discharges were not available, which would have served as a reference for the elaboration of the reservoir operation model and for the definition of the objectives of optimization, reducing some assumptions.

Future works in this area are recommended to evaluate different multi-objective optimizers and ML models. For the Hatillo reservoir, new objectives can be included such as firm energy, or the flow regime alteration downstream of the dam. Further, if the necessary information were available, the models could be expanded to include economic variables that allow the reservoir's operation to be evaluated directly in terms of decision-making costs. Likewise, the performance of the operation models incorporating forecasting reservoir inflows, as well as the incorporation of rainfall data as input variables, should be evaluated. It would also be contemplated to evaluate different scenarios including possible changes in the components of the system, such as the increase in its installed hydropower capacity. Finally, future research could evaluate different optimization formulation for different seasons (i.e., dry seasons or wet seasons).

Acknowledgments

The authors acknowledge the information provided by Dominican Institute of Water Resources (INDHRI) and Empresa de Generación Eléctrica Dominicana (EGEHID) who supplied the data about the reservoir operation. The authors also acknowledge MESCYT in the Dominican Republic, for the research grant awarded to PUCMM (FONDOCYT # 2015-1H2-107) that led to the project in the Yuna river basin.

References

Ahmed, J. A., & Sarma, A. K. (2007). Artificial neural network model for synthetic streamflow generation. Water Resour Manage, 21, 1015–1029, doi:10.1007/s11269-006-9070-y.

Basu, M. (2004). Goal-Attainment Method Based on Simulated Annealing Technique for Economic-Environmental-Dispatch of Hydrothermal Power Systems with Cascaded Reservoirs. Electric Power Components and Systems, 32(12), 1269-1286, doi:10.1080/15325000490446692.

Benítez-Hidalgo, A., Nebro, A., García-Nieto, J., & Oregi, I. (December 2019). jMetalPy: A Python framework for multi-objective optimization with metaheuristics. Swarm and Evolutionary Computation., 51, 100598, doi:10.1016/j.swevo.2019.100598.

Berge, D., Almanzar, L., & Bækken, T. (2003). Environmental Impact Assessment of the Alto Yuna. Oslo, Norway: NIVA.

Cámara, D. (2015). Evolution and Evolutionary Algorithms. In: Bio-inspired Networking. Elsevier, doi:10.1016/B978-1-78548-021-8.50001-6.

Castelletti, A., Pianosi, F., Quach, X., & Soncini-Sessa, R. (2012). Assessing water resources management and development in Northern Vietnam. Hydrology and Earth System Sciences Discussions, 16, 189–199, doi:10.5194/hess-16-189-2012.

CEPAL. Naciones Unidas. (2008). Evolución del impacto de la tormenta Noel en República Dominicana. México: LC/MEX7L.853.

CEPAL. (2020). Análisis espacial de datos históricos y escenarios de cambio climático en México, Centroamérica, Cuba, Haití y la República Dominicana. México: LC/MEX/TS.2020/43.

Chollet, F. K. (2015). Keras. GitHub. Retrieved from https://github.com/fchollet/keras.

Corzo Perez, G. A. (2009). Hybrid models for hydrological forecasting: Integration of data-driven and conceptual modelling techniques. IHE Delft Institute for Water Education.

Deb, K., Pratap, A., Agarwal, S., & Meyarivan. (2002). A Fast and Elitist Multiobjective Genetic Algorithm: NSGA-II. IEEE Transactions on Evolutionary Computation, 6(2), 182-197, doi:10.1109/4235.996017.

Ehsani, N., Fekete, B. M., Vörösmarty , C. J., & Tessler, Z. D. (2016). A neural network based general reservoir operation scheme. Stochastic Environmental Research and Risk Assessment, 30(4), 1151–1166, doi:10.1007/s00477-015-1147-9.

Emanueli Gandara, C. (2017). Exploring spatial-temporal data driven modelling techniques for flow forecasting. UNESCO-IHE. https://cdm21063.contentdm.oclc.org/digital/collection/masters2/id/104820.

Gembicki, F., & Haimes, Y. (1975). Approach to performance and sensitivity multiobjective optimization: The goal attainment method. IEEE Transactions on Automatic Control, 20(6), 769-771, doi:10.1109/TAC.1975.1101105.

Giuliani, M., Castelletti, A., Pianosi , F., Mason, E., & Reed, P. M. (2016). Curses, Tradeoffs, and Scalable Management: Advancing Evolutionary Multiobjective Direct Policy Search to Improve Water Reservoir Operations. ASCE, Journal of Water Resources Planning and Management, 142, 04015050-1 - 04015050-17, doi:10.1061/(ASCE)WR.1943-5452.0000570.

Giuliani, M., Herman, J. D., Castelletti, A., & Reed, P. (2014). Many-objective reservoir policy identification and refinement to reduce policy inertia and myopia in water management. (AGU, Ed.) Water Resources Research, 50, 3355-3377, doi:10.1002/2013WR014700.

Haimes YY, Lasdon LS, & Wismer DA. (1971). On a bicriterion formulation of the problems of integrated system identification and system optimization. IEEE Trans. Syst. Man Cybern, 1(3), 296-297, doi:10.1109/TSMC.1971.4308298.

Heydari, M., Othman, F., & Taghieh, M. (2016). Optimization of Multiple and Multipurpose Reservoir System Operations by Using Matrix Structure (Case Study: Karun and Dez Reservoir Dams). PLOS ONE, 11(6), e0156276, doi:org/10.1371/journal.pone.0156276

Jansen, L., Lariyah, S., Mohamed, D., & Pierre, J. (2013). Hydropower Reservoir for Flood Control: A Case Study on Ringlet Reservoir, Cameron Highlands, Malaysia. Journal of Flood Engineering, 4(1), 87-109.

Jesús Encarnación, A. (2019). Planteamiento de plan de emergencia de las presas del complejo Nizao (República Dominicana), frente a los fenómenos climáticos extremos. Valencia: Universitat Politècnica de València.

Jury, M., Malmgren, B., & Winter, A. (2007). Subregional precipitation climate of the Caribbean and relationships with ENSO and NAO. Journal of Geophysical Research, 112, D16107, doi:org/10.1029/2006JD007541.

Khattab, M., & Al-Mohseen, K. (2020). Planning and Decision Making Under Uncertainty (Mosul Reservoir Optimal Operating Policy - Case Study). Al-Rafidain Engineering Journal, 25, 85-96, doi:10.33899/rengj.2020.126885.1032.

Ko, S.-K., Fontane, D. G., & Labadie, J. W. (1992). Multiobjective Optimization of Reservoir Systems Operation. Water Resources Bulletin, 28(1), 111-27, doi:org/10.1111/j.1752-1688.1992.tb03158.x.

Kollat, J., Reed, P., & Maxwell, R. (2011). Many-objective groundwater monitoring network design using bias-aware ensemble Kalman filtering, evolutionary optimization, and visual analytics. Water Resources Research, 47, W02529, doi:10.1029/2010WR009194.

Koutsoyiannis, D., & Economou, A. (2003). Evaluation of the parameterization-simulation-optimization approach for the control of reservoir systems. Water Resources Research, 39(6), 1170. doi:10.1029/2003WR002148.

Labadie, J. W. (2004). Optimal operation of multireservoir systems: State-of-the-art review. Journal of Water Resources Planning and Management, 130(2), 93-111. doi:10.1061/(ASCE)0733-9496(2004)130:2(93).

Loucks, D., & van Beek, E. (2017). Data-Fitting, Evolutionary, and Qualitative Modeling. In: Water Resource Systems Planning and Management. Gewerbestrasse, Switzerland: Springer. doi:10.1007/978-3-319-44234-1_5.

Ma, X., Liu, F., Qi, Y., Li, L., Jiao, L., Deng, et al. (2015). MOEA/D with biased weight adjustment inspired by user preference and its application on multi-objective reservoir flood control problem. Soft Computing, 20(12), 4999-5023, doi:10.1007/s00500-015-1789-z.

MEPyD. (2017). Pérdidas provocadas por los fenómenos naturales entre noviembre 2016 y septiembre 2017. Santo Domingo: MINISTERIO DE ECONOMÍA, PLANIFICACIÓN Y DESARROLLO.

Miettinen , K. (1999). Nonlinear Multiobjective Optimization. Springer, Boston, MA.

Momtahen, S., & Dariane, A. (2007). Direct Search Approaches Using Genetic Algorithms for Optimization of Water Reservoir Operating Policies. ASCE, Journal of Water Resources

Planning and Management, 133(3), 202-209, doi:10.1061/(ASCE)0733-9496(2007)133:3(202).

Moquete, C. (2004). *Generalidades del Cultivo de Arroz.* Santo Domingo: IDIAF.

Myo Lin, N., & Rutten, M. (2016). Optimal Operation of a Network of Multi-purpose Reservoir: A Review. Procedia Engineering, 154, 1376-1384, doi:10.1016/j.proeng.2016.07.504.

Myo Lin, N., Tian, X., Rutten, M., Abraham, E., Maestre, J. M., & van de Giesen, N. (2020). Multi-Objective Model Predictive Control for Real-Time Operation of a Multi-Reservoir System. Water, 12(7), 1898, doi:10.3390/w12071898.

National Oceanic and Atmospheric Administration. (2015). Oscillation Nino index signal (ONI). Retrieved Julio 15, 2020, from https://origin.cpc.ncep.noaa.gov/products/analysis_monitoring/ensostuff/ONI_v5.php.

Pedregosa, F., Varoquaux, G., Gramfort, A., Michel , V., Thirion, B., Grisel, O., et al.(2011). Scikit-learn: Machine Learning in Python. Journal of Machine Learning Research, 12(2011), 2825-2830.

Ritter, J. (2016). Optimization of hydropower dam cascade operations with respect to energy generation, flood hazard and flow regime alteration, using operational modelling: a case study in the Nechí catchment. Delf: UNESCO-IHE.

Ritter, J., Corzo, G., Solomatine, D. P., & Angarita, H. (2020). Multiobjective Direct Policy Search Using Physically Based Operating Rules in Multireservoir Systems. Journal of Water Resources Planning and Management, 146(4), 05020002, doi:10.1061/(ASCE)WR.1943-5452.0001159.

Rosenstein, M., & Barto, A. (2001). Robot Weightlifting by Direct Policy Search. Seventeenth International Joint Conference on Artificial Intelligence, 2, 839-844.

Ruijie, Z., Cai, X., Ringler, C., & Zhu, T. (2017). Hydropower versus irrigation - an analysis of global patterns. Enviromental Research Letters, 12, 034006, doi:org/10.1088/1748-9326/aa5f3f.

Saavedra, O. C., Koike, T., Yang, K., & Yang, D. (2010). Optimal Dam Operation during Flood Season Using a Distributed Hydrological Model and a Heuristic Algorithm. *Journal of Hydrologic Engineering ASCE*, 15(7), 580-586, doi:10.1061/(ASCE)HE.1943-5584.0000212.

Scola, L., Takahashi, R. H., & Cerqueira, S. (2014). Multipurpose Water Reservoir Management: An Evolutionary Multiobjective Optimization Approach. Mathematical Problems in Engineering, 2014(638259), 14, doi:org/10.1155/2014/638259.

Smith, M. (1992). CROPWAT: a computer program for irrigation planning and management. Rome: Food and Agriculture Organization of the United Nations.

Sun, X., Luo, J., & Xie, J. (2018). Multi-objective Optimization for Reservoir Operation Considering Water Diversion and Power Generation Objectives. Water, 10, 1540, doi:org/10.3390/w10111540.

Tami, C. (2020). Identificación de reglas de operación óptimas de embalses para el control de inundaciones a partir de modelos de operación. Caso de estudio: Cuenca del Río Yuna en República Dominicana. Bogotá D.C: Escuela Colombiana de Ingeniería. https://repositorio.escuelaing.edu.co/handle/001/1290.

Tikk, D., Kóczy, L., & Gedeon, T. (2003). A survey on universal approximation and its limits in soft computing techniques. International Journal of Approximate Reasoning, 33(2), 185-202, doi:10.1016/S0888-613X(03)00021-5.

Viparelli, R. (1983). Spillways for Multipurpose Reservoirs, to Regulate the Runoff available at the Dam Section and For the Control of Floods. International Conference on the Hydraulics Aspects of Floods & Flood Controls (págs. 109-128). London, England: City, University of London.

Zhang, D., Lin, J., Peng, Q., Wang, D., Yang, T., Sorooshian, S., et al. (2018). Modeling and simulating of reservoir operation using the artificial neural network, support vector regression, deep learning algorithm. ELSEVIER, Journal of Hydrology, 565, 720–736, doi:10.1016/j.jhydrol.2018.08.050.

Zhang, Q., & Li, H. (2007). MOEA/D: A Multiobjective Evolutionary Algorithm Based on Decomposition. IEEE Transactions on Evolutionary Computation, 11(6), 712-731, doi:10.1109/TEVC.2007.892759.

Zhou, C., Sun, N., Chen, L., Ding, Y., Zhou, J., Zha, G., et al. (2018). Optimal Operation of Cascade Reservoirs for Flood Control of Multiple Areas Downstream: A Case Study in the Upper Yangtze River Basin. Water, 10, 1250, doi:10.3390/w10091250.